J|A|C|S
ARTICLES
Published on Web 01/30/2004

Protons in Supercritical Water: A Multistate Empirical Valence Bond Study

Daniel Laria,*,† Jordi Martí, and Elvira Guàrdia

Contribution from the Departament de Física i Enginyeria Nuclear, Universitat Politècnica de Catalunya, B4-B5 Campus Nord, 08034 Barcelona, Spain

Received July 17, 2003; E-mail: dhlaria@cnea.gov.ar

Abstract: Molecular dynamics simulations have been performed to analyze microscopic details related to aqueous solvation of excess protons along the supercritical $T = 673$ K isotherm, spanning a density interval from a typical liquid down to vapor environments. The simulation methodology relies on a multistate empirical valence bond Hamiltonian model that includes a proton translocation mechanism. Our results predict a gradual stabilization of the solvated Eigen cation $[H_3O\cdot(H_2O)_3]^+$ at lower densities, in detriment of the symmetric Zundel dimer $[H\cdot(H_2O)_2]^+$. At all densities, the average solvation structure in the close vicinity of the hydronium is characterized by three hydrogen bond acceptor water molecules and presents minor changes in the solute water distances. Characteristic times for the proton translocation jumps have been computed using population relaxation time correlation functions. Compared to room temperature results, the rates at high densities are 4 times faster and become progressively slower in steamlike environments. Diffusion coefficients for the excess proton have also been computed. In agreement with conductometric data, our results show that contributions from the Grotthus mechanism to the overall proton transport diminish at lower densities and predict that in steamlike environments, the proton diffusion is almost 1 order of magnitude slower than that for pure water. Spectroscopic information for the solvated proton is accordant to the gradual prevalence of proton localization in Eigen-like structures at lower densities.

Introduction

Protons represent a ubiquitous species in aqueous solutions and play a key role controlling many processes of fundamental importance in both chemistry and biology, such as acid−base equilibria and charge transport across biological membranes.[1,2] In the past and despite its apparent simplicity, the microscopic nature of the solvated proton raised several controversial issues[3−6] that have found appropriate interpretations only in recent times. For example, one important question to be answered was whether the prevailing microscopic solvation structure for the excess charge would correspond to the Zundel dimer[7] $[H\cdot(H_2O)_2]^+$ or the Eigen cation[8] $[H_3O\cdot(H_2O)_3]^+$. At present, there seems to be sufficient evidence that these complexes actually represent limiting structures and that the most appropriate picture for the hydrated proton is that of a fluxional defect immersed in the hydrogen-bonded network of liquid water, whose dynamics is very much controlled and modulated by that of the hydrogen bonding in the host liquid.[9]

From the dynamical point of view, perhaps the most striking feature that distinguishes aqueous protons from the rest of simple cations is its abnormally large mobility. In 1806, Grotthus introduced the idea of a mechanism for the transport which does not involve the individual diffusion of a tagged proton;[10] instead, it would require successive spatial rearrangements along chains of hydrogen bonds, resulting in a translocation of the average position of the excess charge over length scales well beyond the size of a water molecule. Surprisingly enough, recent ab initio molecular dynamics simulations have confirmed the validity of this picture, which was postulated almost two centuries ago.[9,11−13]

Bearing in mind this picture, it is interesting to speculate about the changes that should take place if one is interested in analyzing the solvation of aqueous protons at elevated temperatures, i.e., above the normal boiling point, with the realm of supercritical (SC) states of water (T > 374 °C) as limiting environments. This subject is of great importance not only in fundamental chemistry but also from a technological point of

† Permanent address: Unidad Actividad Química, CNEA, and Departamento de Química Inorgánica Analítica y Química Física, Universidad de Buenos Aires, Argentina.

(1) *Electron and Proton Transfer in Chemistry and Biology*. Muller, A., Ratajczak, H., Junge, W., Diemann, E., Eds.; Elsevier: New York, 1992.
(2) Jefreey, G. A.; Saenger, W. *Hydrogen Bonding in Biological Structures*; Springer: Berlin, 1994.
(3) Hückel, E. *Z. Elektrochem.* **1928**, *34*, 546.
(4) Bernal, J. D.; Fowler, R. H. *J. Chem. Phys.* **1933**, *1*, 515.
(5) Bell, R. P. *The Proton in Chemistry*; Cornell University Press: Ithaca, NY, 1973.
(6) Caldin, E. F.; Gold, V. *Proton-Transfer Reactions*; Chapman and Hall: London, 1975.
(7) Zundel, G.; Metzger, H. *Z. Phys. Chem.* **1968**, *244*, 456.
(8) Eigen, M.; de Maeyer, L. *Proc. R. Soc. London* **1958**, *A247*, 505.
(9) (a) Marx, D.; Tuckerman, M. E.; Hutter, J.; Parrinello, M. *Nature* **1999**, *397*, 601. (b) Tuckerman, M. E.; Marx, D.; Parrinello, M. *Nature* **2002**, *417*, 925.
(10) von Grotthus, C. J. D. *Ann. Chim.* **1806**, *LVIII*, 54.
(11) Tuckerman, M.; Laasonen, K.; Sprik, M.; Parrinello, M. *J. Chem. Phys.* **1995**, *103*, 150.
(12) Tuckerman, M.; Laasonen, K.; Sprik, M.; Parrinello, M. *J. Phys. Chem.* **1995**, *99*, 5794.
(13) Marx, D.; Tuckerman, M. E.; Parrinello, M. *J. Phys.: Condens. Matter* **2000**, *12*, A153.

view, since the control of many hydrothermal processes such as oxidation for safe disposal of hazardous organic wastes as well as corrosion, catalytic, precipitation, and hydrolysis processes is very much dependent on the pH prevailing in the environment.[14,15]

In this context, one important modification that operates in high-temperature water is the drastic drop in its macroscopic dielectric constant, down to a value of ~6 at near critical conditions. Consequently, one could anticipate that these changes in the solvent polarity should be translated into nonnegligible shifts in chemical equilibria and absorption line shapes involving ionic species. We bring into consideration as one clear example recent spectroscopic measurements of aqueous solutions of H_2SO_4 that show that the strength of the acid decreases considerably as one surpasses $T \approx 350$ °C.[16] Of course, the drop in water polarity reflects important changes in its microscopic structure, most notably those involving the architecture of the hydrogen bond network. Although the degree of persistence of hydrogen bonding in SC water is still subjected to some uncertainty,[17] the modifications in the structure of water are sufficiently strong so as to affect the equilibrium aspects of proton solvation in a sensible way.

From the dynamical side, one should also expect important alterations since collective and single particle orientational modes in SC water are normally faster at lower densities;[18−26] these modes affect the kinetics of hydrogen bonding[27] and, indirectly, should also alter the rates for proton transfer.[28,29] Coming back to the subject of proton diffusion, one fundamental question that still requires appropriate interpretation is establishing which modifications in the microscopic mechanism drive the proton transport at elevated temperatures compared to what is normally perceived at ambient conditions. This problem is intimately connected to that of ionic transport in high-temperature aqueous solutions, a subject that has received a great deal of attention in recent times.[30−33] The physical picture that emerges from these studies suggests that ionic mobility in supercritical water is the result of a complex interplay in which intervene in a non trivial fashion not only structural, but also dynamical effects such as viscous and dielectric friction. As a result, the mobility of simple ionic species may present nonuniform, and even nonmonotonic, density dependence.[32] Given this scenario, one would expect the analysis of the transport of aqueous protons at elevated temperatures to be even more complex since it should include some extent of the "structural charge defect" transport mechanism present at ambient conditions, in addition to the usual hydrodynamic Stokes mass diffusion.

The previous paragraph has underlined the importance of the main objective of this paper in which we present the first microscopic approach to equilibrium and dynamical aspects of the solvation of hydrated protons at SC conditions from a molecular dynamics perspective. To that end, we performed a series of computer simulation experiments along the $T = 673$ K isotherm. To differentiate temperature from density effects, we spanned a wide interval of solvent densities, ranging from highly packed fluids, $\rho_w = 1$ g cm^{-3}, to typical steamlike environments, $\rho_w = 0.1-0.05$ g cm^{-3}. The former state corresponds to water at extreme pressures (~0.7−0.8 GPa), while the latter interval corresponds to that prevailing in most technological applications. To tackle the problem, we adopted a methodology based on an extended empirical valence bond (EVB) model Hamiltonian. This approach has been successfully implemented in analyzing proton solvation in water at ambient conditions.[34−45] One interesting feature of this methodology is that it can incorporate quantum fluctuations arising from the light nature of the proton. This has been carried out using a reparametrization of the potential energy surface based on a path integral representation of the quantum proton[42] or instead, by resorting to centroid molecular dynamics methods.[34,46] However, at this stage we made no efforts either to look for possible improvements of the performance of the Hamiltonian at higher temperatures or to explicitly incorporate quantum effects in the simulation experiments. Although the latter does modify the equilibrium solvation structures and dynamics, the resulting trends do not substantially differ from those obtained classically.[36] Instead, we concentrated attention on the gross features and qualitative changes that take place in well-differentiated supercritical states, ranging from highly packed fluids to vapor environments. In addition, we managed to establish a proper comparison between our results at elevated temperatures

(14) Holgate, J. W.; Armellin, H. R.; Webley, P. A.; Killilea, W. R.; Hong, G. T.; Barner, H. E. In *Emerging Technologies in Hazardous Waste Management III*; Tedder, D. W., Pohland, F. G., Eds.; American Chemical Society: Washington, DC, 1993.
(15) *Physical Chemistry of Aqueous Systems: Meeting the Needs of Industry*; White, J. H., Sengers, J. V., Neumann, D. B., Bellows, J. C., Eds.; Begell House: New York, 1994.
(16) Xiang, T.; Johnston, K. P.; Wofford, W. T.; Gloyna, E. F. *Ind. Eng. Chem. Res.* **1996**, *35*, 4788.
(17) For articles for and against the existence of hydrogen bonding in SC water, see refs 18−24.
(18) (a) Postorino, P.; Tromp, R. H.; Ricci, M.-A.; Soper, A. K.; Neilson, G. W. *Nature* **1993**, *366*, 668. (b) Postorino, P.; Ricci, M.-A.; Soper, A. K. *J. Chem. Phys.* **1994**, *101*, 4123.
(19) (a) Gorbaty, Y. E.; Kalinichev, A. G. *J. Phys. Chem.* **1995**, *99*, 5336. (b) Kalinichev, A. G.; Bass, J. D. *J. Phys. Chem. A* **1997**, *101*, 9720.
(20) Ikushima, Y.; Hatakeda, K.; Satio, N.; Masahiko, A. *J. Chem. Phys.* **1998**, *108*, 5855.
(21) Frank, E. U.; Roth, K. *Discuss. Faraday Soc.* **1967**, *63*, 108.
(22) Hoffman, M. M.; Conradi, M. S. *J. Am. Chem. Soc.* **1997**, *119*, 3811.
(23) Soper, A. K.; Bruni, F.; Ricci, M.-A. *J. Chem. Phys.* **1997**, *106*, 247.
(24) Jedlovsky, P.; Vallauri, R. *J. Chem. Phys.* **1996**, *105*, 2391.
(25) Skaf, M. S.; Laria, D. *J. Chem. Phys.* **2000**, *113*, 3499.
(26) Re, M.; Laria, D. *J. Phys. Chem. B* **1997**, *101*, 10494.
(27) Martí, J. *Phys. Rev. E* **2000**, *61*, 449.
(28) Agmon, N. *J. Phys. Chem.* **1996**, *100*, 1080.
(29) Cohen, B.; Hupper, D. *J. Phys. Chem. A* **2003**, *107*, 3598.
(30) (a) Koneshan, S.; Rasaiah, J. C.; Lynden-Bell, R. M.; Lee, S. H. *J. Phys. Chem. B* **1998**, *102*, 4193. (b) Noworyta, J.; Koneshan, S.; Rasaiah, J. C. *J. Am. Chem. Soc.* **2000**, *122*, 11194. (c) Rasaiah, J. C.; Noworyta, J.; Koneshan, S. *J. Am. Chem. Soc.* **2000**, *122*, 11182. (d) Koneshan, S.; Rasaiah, J. C. *J. Chem. Phys.* **2000**, *113*, 8125. (e) Koneshan, S.; Rasaiah, J. C.; Dang, L. X. *J. Chem. Phys.* **2001**, *114*, 7544.
(31) Lee, S. H.; Cummings, P. T. *J. Chem. Phys.* **2000**, *112*, 864.
(32) Balbuena, P.; Johnston, K.; Rossky, P. J. *J. Phys. Chem.* **1996**, *100*, 2706.
(33) Hyun, J.-K.; Johnston, K. P.; Rossky, P. J. *J. Phys. Chem. B* **2001**, *105*, 9302.
(34) Lobaugh, J.; Voth, G. A. *J. Chem. Phys.* **1996**, *104*, 2056.
(35) Schmitt, U. W.; Voth, G. A. *J. Chem. Phys. B* **1998**, *102*, 5547.
(36) Schmitt, U. W.; Voth, G. A. *J. Chem. Phys.* **1999**, *111*, 9361.
(37) Day, T. J. F.; Schmitt, U. W.; Voth, G. A. *J. Am. Chem. Soc.* **2000**, *122*, 12027.
(38) Day, T. J. F.; Soudackov, A. V.; Cuma, M.; Schmitt, U. W.; Voth, G. A. *J. Chem. Phys.* **2002**, *117*, 5839.
(39) Vuilleumier, R.; Borgis, D. *J. Phys. B* **1998**, *102*, 4261.
(40) Vuilleumier, R.; Borgis, D. *Chem. Phys. Lett.* **1998**, *284*, 71.
(41) Vuilleumier, R.; Borgis, D. In *Classical and Quantum Dynamics in Condensed Phase Simulations*; Berne, B. J., Ciccotti, G., Coker, D. F., Eds.; World Scientific: Singapore, 1998; Chapter 30.
(42) Vuilleumier, R.; Borgis, D. *J. Chem. Phys.* **1999**, *111*, 4251.
(43) Sagnella, D. E.; Tuckerman, M. E. *J. Chem. Phys.* **1998**, *108*, 2073.
(44) Kornyshev, A. A.; Kuznetsov, A. M.; Spohr, E.; Ulstrup, J. *J. Phys. Chem. B* **2003**, *107*, 3351.
(45) Walbran, S.; Kornyshev, A. A. *J. Chem. Phys.* **2001**, *114*, 10039.
(46) The implementation of centroid molecular dynamics techniques is described in detail in: (a) Cao, J.; Voth, G. A. *J. Chem. Phys.* **1993**, *99*, 10070. (b) Cao, J.; Voth, G. A. *J. Chem. Phys.* **1994**, *100*, 5093. (c) Cao, J.; Voth, G. A. *J. Chem. Phys.* **1994**, *100*, 5106. (d) Cao, J.; Voth, G. A. *J. Chem. Phys.* **1994**, *101*, 6157.

and those obtained at ambient conditions using a similar Hamiltonian.[36−38]

The organization of the present work is as follows. In the next section, we present an overview of the model and the simulation procedure. The central part of the paper is devoted to the simulation results and includes a description of the equilibrium solvation structures and dynamical information pertaining to the rate of proton transfer and also to the proton transport. In addition, we briefly analyze temperature and density effects on the infrared absorption spectra. The concluding remarks are summarized in the last section.

Model and Simulation Procedure

The computer simulations presented in this study were performed using an EVB approach. The implementation of this methodology to study chemical reactivity has been described extensively in the literature;[47−50] therefore, for the sake of concision, we will restrict our presentation to the main features.

The basic idea is conceptually simple and assumes that the Born−Oppenheimer potential energy surface $\epsilon_0(\{\mathbf{R}\})$ that drives the dynamics of the nuclei with coordinates $\{\mathbf{R}\}$ can be obtained from the lowest instantaneous eigenvalue of the following EVB Hamiltonian:

$$\hat{H}_{EVB}(\{\mathbf{R}\}) = \sum_{ij} |\phi_i\rangle h_{ij}(\{\mathbf{R}\}) \langle\phi_j| \tag{1}$$

In the previous equation, we have chosen a representation of the EVB Hamiltonian in terms of the basis set $\{|\phi_i\rangle\}$ of diabatic valence bond (VB) states. For the particular case of an excess proton in water, these diabatic states designate configurations with the H^+ located in a particular water molecule. The ground state $|\psi_0\rangle$ of $\hat{H}_{EVB}$ satisfies:

$$\hat{H}_{EVB}|\psi_0\rangle = \epsilon_0(\{\mathbf{R}\})|\psi_0\rangle \tag{2}$$

and can be expanded as a linear combination of diabatic states as:

$$|\psi_0\rangle = \sum_i c_i |\phi_i\rangle \tag{3}$$

leading to the final expression for the potential energy surface:

$$\epsilon_0\{\mathbf{R}\} = \sum_{ij} c_i c_j h_{ij}(\{\mathbf{R}\}) \tag{4}$$

The dynamics of the nuclei of mass M_k is governed by the following Newton's equation:

$$M_k \frac{d^2\mathbf{R}_k}{dt^2} = -\sum_{ij} c_i c_j \nabla_{\mathbf{R}_k} h_{ij}(\{\mathbf{R}\}) \tag{5}$$

One of the features of EVB methods is that the different matrix elements h_{ij} can be cast in terms of the different nuclear coordinates to agree with results from very precise quantum calculations. The parametrization adopted here was similar to that proposed by Schmitt and Voth.[36,51] Diagonal elements h_{ii} comprise contributions from stretching and bending intramolecular interactions within the tagged H_3O^+ and in the rest of the water molecules, which are modeled using the flexible TIP3P mean field model.[52] In addition, the diagonal elements include hydronium−solvent and solvent−solvent intermolecular interactions. The off-diagonal elements h_{ij} introduce the coupling between the diabatic states i and j and were modeled to include interatomic contributions within the particular $(H_5O_2)^+$ dimer spanned by states $|\phi_i\rangle$ and $|\phi_j\rangle$ and also exchange Coulombic interactions between the dimer and the rest of the solvent. The complete list of the parameters can be found in ref 36. Within this level of approximation, Schmitt and Voth were able to reproduce geometries and energetics of some relevant protonated water clusters obtained with sophisticated ab initio methods of electronic structure calculations.

The systems under investigation were composed by one proton dissolved in 125 water molecules. All simulation experiments corresponded to microcanonical runs at temperatures $T = 673 \pm 20$ K; the water densities examined were $\rho_w = 0.05$, 0.1, 0.3, 0.65, and 1 g cm^{-3}. The time step was set to $\Delta t = 0.5$ fs; all simulations included an equilibration period of approximately 20 ps, followed by trajectories of typically ∼500 ps that were used to evaluate the statistical properties of the systems. Long-range interactions derived from the different Coulombic terms were handled by Ewald sum techniques[53] by assuming the presence of a uniform neutralizing background.

The construction of the EVB Hamiltonian was performed as follows.[36,42] First, it required the insertion of the excess proton within a cavity in a previously equilibrated water sample as well as the identification of the water molecule closest to the excess proton. This fixed the initial H_3O^+ pivot and the first diabatic state. From this pivot, the rest of the diabatic states were chosen in a treelike construction, via a hydrogen-bond connectivity pattern. The wide range of investigated solvent densities led us to impose a slightly modified criterion, from the one proposed in ref 36, to establish a hydrogen bond. The maximum oxygen acceptor−proton donor distance was relaxed up to 2.8 Å; in addition, we supplemented it with a geometrical restriction, imposing a minimum threshold value of the H−O···O angle of 30°. All molecules lying in and up to the third solvation shell, showing a connecting path with the original pivot, were included in the construction of the $L \times L$, EVB Hamiltonian matrix. With this procedure, the size of the Hamiltonian matrix varied from $L \approx 20$ at high solvent densities, down to $L \approx 10$ for low-density states. The resulting dynamics was stable over the complete lengths of the simulation runs, with fluctuations in the total energy that never surpassed 1%. At each step, proton transfer was made possible by reassigning the pivot oxygen label to the instantaneous state exhibiting the largest c_i^2. From this state, the list of participating VB states was reconstructed using the connectivity branching procedure mentioned above.

Results

Microscopic Solvation of H^+. The presence of an excess proton in bulk water promotes a disruption in the original structure of hydrogen bonds in the neat liquid. At present, the most widely accepted microscopic picture of the proton aqueous solvation involves a whole series of intermediate structures between those of the two limiting cations: the three-coordinated hydronium $[H_3O\cdot(H_2O)_3]^+$ known as the Eigen cation[8] and the symmetric Zundel dimer[7] $[H\cdot(H_2O)_2]^+$. Along a typical simulation run, one normally observes a continuous interconversion between the two structures generating a *hybrid* $(H_9O_4)^+/(H_5O_2)^+$ complex;[9,12] such interconversions take place typically in the picosecond time scale and involve slight displacements in the relevant O−O distances as well as subtle changes in the hydrogen connectivity pattern between the complex and the nearest solvation shell.

(47) Coulson, C. A.; Danielsson, U. *Ark. Fys.* **1954**, *8*, 239.
(48) Mulliken, R. S. *J. Chem. Phys.* **1964**, *61*, 20.
(49) Aqvist, J.; Warshel, A. *Chem. Rev.* **1993**, *93*, 2523.
(50) Warshel, A. *Computer Modeling of Chemical Reactions in Enzymes and Solutions*; Wiley: New York, 1980.
(51) Recently, a new parametrization of the EVB Hamiltonian has been developed by Voth's group (see ref 38) Although this new model can be applied to the analysis of more complex environments beyond aqueous systems, results for the aqueous proton are similar to those published in ref 36.
(52) Dang, L. X.; Pettit, B. M. *J. Chem. Phys.* **1987**, *91*, 3349.
(53) Allen, M. P.; Tildesley, D. J. *Computer Simulation of Liquids*; Clarendon Press: Oxford, 1997.

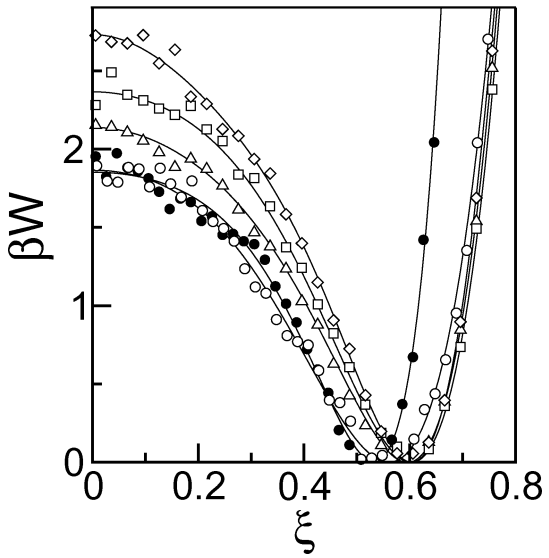

Figure 1. Free energy associated with the asymmetric order parameter ξ (see text) for aqueous excess protons at different thermodynamic states along the $T = 673$ K isotherm. $\rho_w = 0.05$ g cm^{-3} (diamonds), $\rho_w = 0.1$ g cm^{-3} (squares), $\rho_w = 0.3$ g cm^{-3} (triangles), and $\rho_w = 1$ g cm^{-3} (open circles). Also shown are results for ambient conditions (black circles). Lines represent least-squares fits and are included as an aid for the eye.

Within the EVB model, the gross features of these structures can be conveniently analyzed by considering the probability densities associated to an appropriate order parameter. Following previous studies,[36,38] we computed:

$$\beta W(\tilde{\xi}) \propto -\ln[\langle \delta(\xi - \tilde{\xi})\rangle] \tag{6}$$

where β is the inverse of Boltzmann constant times the temperature and $\langle ....\rangle$ represents a statistical average. $W(\xi)$ is the free energy associated with the probability distribution of the asymmetric order parameter defined as:

$$\xi = c_1^2 - c_2^2 \tag{7}$$

c_1 and c_2 represent the two largest coefficients of the expansion of the ground state of the Hamiltonian shown in eq 3. Eigen and Zundel structures are characterized by values of ξ close to 1 and 0, respectively. Profiles of $W(\xi)$ are depicted in Figure 1. Regardless of the temperature considered, Eigen cations in high-density fluids are characterized by similar values of the order parameter $\xi \approx 0.52$. A moderate shift toward $\xi \approx 0.60$ appears as we move to lower densities. Thermal effects become more evident as one inspects the widths of the distributions, the supercritical ones being somewhat broader than those corresponding to room temperature. For the former cases, there seems to be a larger number of thermally accessible states exhibiting $\xi \gtrsim 0.6$, i.e. configurations in which the proton is mainly localized in one individual VB state.

A reasonable estimate for the prevalence of either limiting structure can be obtained from the equilibrium constant K_{eq}, computed from the following ratio of partition functions:

$$K_{eq} = \frac{x_E}{x_Z} = \frac{\int_{\xi^*}^{\infty} \exp(-\beta W(\xi))\, d\xi}{\int_0^{\xi^*} \exp(-\beta W(\xi))\, d\xi} \tag{8}$$

where x_E and $x_Z = 1 - x_E$ represent the equilibrium concentrations of Eigen and Zundel species, respectively. ξ^* represents a value of the order parameter that characterizes the boundary between Eigen from Zundel species and was located at the mean value of the inflection points of all the free energy curves, $\xi^* = 0.45$. In the second and third columns of Table 1, we present estimates for the equilibrium constants and x_E, respectively. At room temperature, approximately 55% of the configurations exhibit Eigen-like characteristics in accordance with ab initio molecular dynamics experiments.[9,12] This proportion increases monotonically as we move up in temperature and down in density, reaching ~75% in the lowest SC density investigated.

Table 1. Equilibrium and Dynamical Properties for the Aqueous H^+ at Different Thermodynamic States along the $T = 673$ K Isotherm[a]

ρ_w	x_E	K_{eq}	τ_{tr}^{-1}	D_{H^+}	D_w	$D^*_{H^+}$
0.05	0.76	3.2	2.4 ± 0.5	6.2 ± 0.4	54.1	7.5
0.1	0.73	2.7	3.6 ± 0.4	5.5 ± 0.8	24.8	5.3
0.3	0.70	2.3	6.8 ± 0.8	3.0 ± 0.8	9.2	2.6
0.65	0.67	2.1	9.7 ± 1.0	2.7 ± 0.7	5.0	1.9
1	0.63	1.7	11.7 ± 1.2	2.6 ± 0.5	2.4	*d*
1[b]	0.55	1.2	3.0[b]	0.45 ± 0.11[b]	0.32[c]	

[a] Densities are expressed in g cm^{-3}; rates in 10^{-1} ps^{-1}; diffusion coefficients in Å^2 ps^{-1}. [b] Results for $T = 300$ K from ref 38. [c] Results fom ref 62. [d] See ref 63.

We now turn to the analysis of the average solvation structure. Given the large disparity in the magnitude of solvent bulk densities covered in this study (a factor of 20 between the highest and the lowest values), we found it more convenient to analyze the microscopic details of the solvation by considering the pivot water local density fields defined as:

$$\rho_{o^*\alpha}(r) = \frac{1}{4\pi r^2} \left\langle \sum_i \delta(|\mathbf{r}_{o^*} - \mathbf{r}_i^{\alpha}| - r) \right\rangle \tag{9}$$

where $\mathbf{r}_{o^*}$ is the coordinate of the instantaneous pivot oxygen and $\mathbf{r}_i^{\alpha}$ denotes the coordinate of site (α = O, H) in the ith solvent molecule.

Spatial correlations with respect to the pivot oxygen are shown in Figure 2. Interestingly, at all the solvent densities considered, the structures of the pivot oxygen profiles shown in the top panel are dominated by the first solvation shells centered at $r = 2.5$ Å—more structured and somewhat narrower at ambient conditions—that include three acceptor water molecules. The fact that, despite the differences in the bulk density, the magnitudes of the main peaks remain comparable reveals that in low-density SC states the proton is able to promote a considerable degree of solvent clustering in its close vicinity. The robustness of the first solvation shell in aqueous supercritical environments has also been corroborated in recent X-ray absorption experiments of aqueous Br^-.[54] The presence of a second shell located at $r = 4.5$ Å is also clearly perceptible in all thermodynamic states investigated, with the exception of the highest supercritical density case ($\rho_w = 1$ g cm^{-3}, $T = 673$ K), where the structure practically vanishes beyond the first peak. These molecules correspond to the second solvation shell of the hydronium, and some of them may act as hydrogen bond acceptors or donors with respect to the inner ones. The analysis of the oxygen pivot hydrogen water profiles shown in the bottom panel provides complementary information. Here, in all cases,

(54) Wallen, S. L.; Palmer, B. J.; Pfund, D. M.; Fulton, J. L.; Newville, M.; Ma, Y.; Stern, E. A. *J. Phys. Chem. A* **1997**, *101*, 9632.

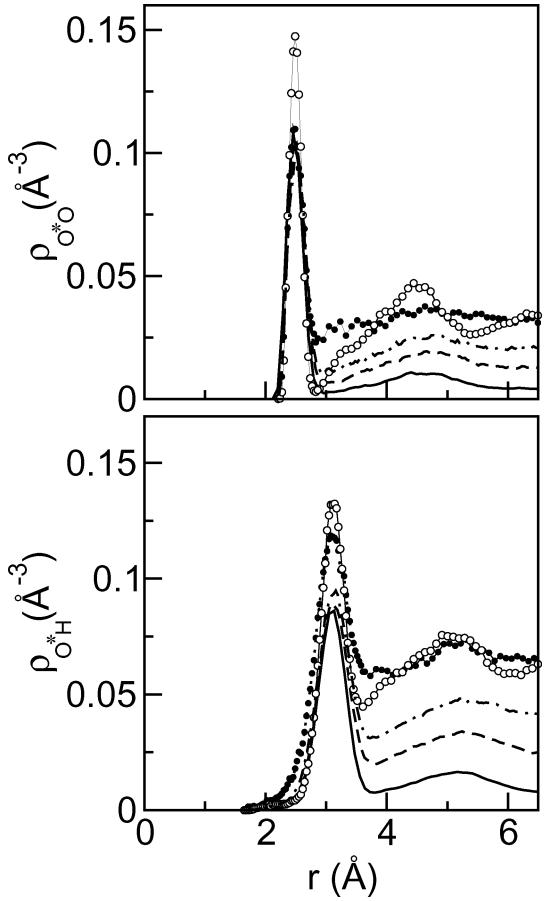

Figure 2. Pivot solvent density fields at different supercritical states of water. $\rho_w = 0.05$ g cm^{-3} (solid lines), $\rho_w = 0.3$ g cm^{-3} (dashed lines), $\rho_w = 0.65$ g cm^{-3} (dot−dashed lines), and $\rho_w = 1$ g cm^{-3} (black circles). Open circles correspond to results for ambient conditions.

we found main peaks located at $r = 3.15$ Å. At low SC densities, these peaks exclusively include the six hydrogen atoms corresponding to the water molecules which belong to the first solvation shell. As the density increases, the number of hydrogen atoms included in the first peak rises to ∼9−11. An analysis of the connectivity of these new hydrogen atoms shows that typically, two of them belong to molecules from the second shell which act as hydrogen bond donors to the inner ones. We finally remark that, regardless of the density and/or temperature investigated, we found no evidence of pivot acceptor hydrogen bonding of the type O−H···O*.

Rates for the Proton Transfer. Perhaps the simplest and most direct route to gain a first insight into the nature of proton transfer dynamics in different aqueous environments is by direct inspection of the time evolutions of the pivot oxygen label that are shown in Figure 3. By simply counting the number of transitions in the three plots, temperature and density effects upon the rate of proton transfer are self-evident: At $T = 300$ K (bottom panel), during the 50 ps temporal interval displayed, approximately 10 water molecules retain the pivot label during periods of of 0.5 ps or longer. That number is at least 4-fold larger, as we move to SC temperatures, keeping the density constant (middle panel). Results for high-temperature, steamlike environments shown in the top panel predict that the number of transitions drops to values comparable to those originally found at ambient conditions. The overall jump patterns, though,

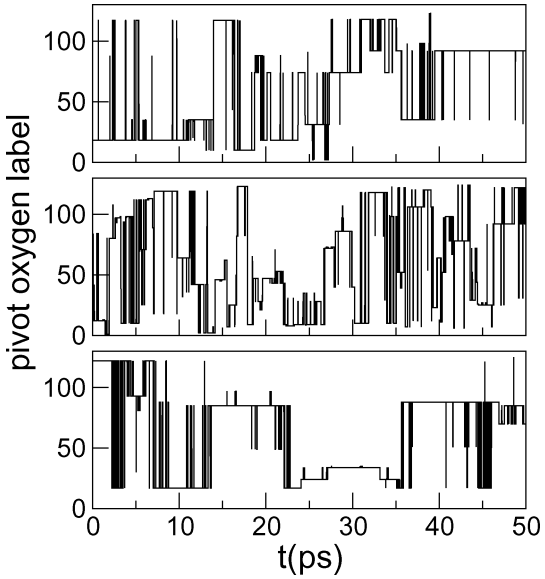

Figure 3. Time evolution of pivot oxygen labeling in different SC aqueous environments ($T = 673$ K). $\rho_w = 0.05$ g cm^{-3} (top panel), and $\rho_w = 1$ g cm^{-3} (central panel). The bottom panel displays results for water at ambient conditions.

look quite similar in the three plots and can be pictured as a sequence of episodes in which the proton resides in one water during a few picoseconds, interrupted by intervals in which the proton resonates rapidly between two VB states, thus establishing what is usually referred to as a "special bond".[11−13,42] A few isolated spikes corresponding to single attempts of aborted transitions complete the description.

The crude picture provided in the previous paragraph can be substantially improved by performing an analysis based on time correlation functions. We remark that in all cases, proton transfers were sufficiently frequent to collect adequate statistics without resorting to special techniques designed to analyze rare event dynamics. Important quantities in this context are the equilibrium time correlation functions for the population relaxations of different reactant species. These functions present the general form:

$$C(t) = \frac{\langle h_i(t) \cdot \delta h_i(0) \rangle}{\langle (\delta h_i)^2 \rangle} \tag{10}$$

where $\delta h_i(t) = h_i(t) - \langle h_i \rangle$ denotes the instantaneous fluctuation of the population of the ith reactant away from its equilibrium value. The characteristic function $h_i(t)$ is unity if the tagged reactant species is present in the system at time t, and zero otherwise. Invoking Onsager's regression hypothesis,[55] the inverse of the proton-transfer rate τ_{tr}^{-1} can be obtained from the temporal decay of $C(t)$ at long time spans.[56]

Population relaxations for the pivot label appear as natural functions to investigate. The previous observations anticipate that the time correlations will have incorporated at least three different time scales: (i) a resonant time in the subpicosecond scale, associated with the rapid alternation of the pivot label along a "special bond", (ii) a second time scale

(55) Chandler, D. In *Introduction to Modern Statistical Mechanics*; Oxford University Press: New York, 1987; Chapter 8.
(56) To establish an appropriate correspondence between the long time relaxation of $C(t)$ and the rate of proton jump, we assumed that $h(t)$ vanishes at all times, following a 0.5 ps time interval in which $h(t)$ is continuously zero.

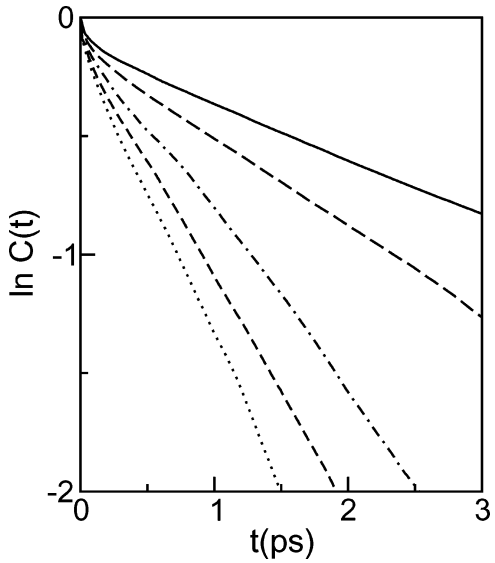

Figure 4. Logarithm of the population relaxations of the pivot label at different SC states of water along the $T = 673$ K isotherm. $\rho_w = 0.05$ g cm^{-3} (solid line), $\rho_w = 0.1$ g cm^{-3} (long-dashed lines), $\rho_w = 0.3$ g cm^{-3} (dot−dashed line), $\rho_w = 0.65$ g cm^{-3} (short-dashed line), and $\rho_w = 1$ g cm^{-3} (dotted line).

characterizing the lifetime of the resonance episodes, and (iii) the largest residence time τ_{tr} of the proton labeling localized in one particular oxygen, which is the relevant time scale characterizing the rate for the proton transfer. Results for the population relaxations of the pivot label over a 4 ps time interval appear in Figure 4. After a 0.5 ps transient—most likely related to the fast processes mentioned above—all curves can be reasonably well described as single exponentials, although we do not discard the possibility of additional slower processes affecting the proton-transfer rate that are not captured in the time interval investigated. Results for the best fits of the decays are listed in the fourth column of Table 1 along with those reported for ambient conditions. It becomes clear that the predicted rates, as reflected by the magnitude of τ_{tr}^{-1}, diminish as we move to lower densities.

The microscopic interpretation of the reduction in the rates requires a careful analysis of the mechanisms that drive the proton transfer. Normally, in adiabatic proton-transfer processes occurring in polar media, one focuses attention on the characteristics of the polarization fluctuations of the environment as the key effects determining the rates.[57,58] For the particular case of aqueous protons, the characterization of such fluctuations is more complex since it is intimately related to the hydrogen bond dynamics. At ambient conditions, there exists evidence that the rate-limiting step for proton transfer in water is the result of a subtle hydrogen bond cleavage occurring in the second solvation shell.[11,12,37,59] In this context, we foresee that important modifications in the reaction mechanism would operate at SC conditions due to at least two factors: (i) the overall shorter lifetime of the hydrogen bonds[27] and (ii) the changes in the solute−solvent and the solvent−solvent spatial and orientational correlations, especially those occurring beyond the first solvation shell. In principle, the rigorous analysis of the connectivity pattern and the characterization of the ensemble of transition states can be performed by appropriate sampling of reactive trajectories.[60] This, though, is well beyond the scope of the present paper, thus, we will not proceed further along this direction. Yet, our results suggest that, similar to what has been reported for ambient conditions, proton transfers in SC environments are not exclusively triggered by solvent polarization fluctuations that make donor and acceptor diabatic states degenerate. Using simple transition state theory arguments, if the bottleneck that separates reactants from product states is characterized by $\xi \approx 0$, one would predict only minor temperature effects on the free energy curves shown in Figure 1, in passing from $T = 300$ K to $T = 673$ K.[61] Note that this argument is not compatible with the observed dynamics. Our results do confirm, however, that the magnitude of the free energy barrier at the corresponding transition states increases as we move toward smaller densities, which in turn, would support the idea of a much more localized proton in steamlike environments.

Table 2. Experimental Diffusion Coefficients of H^+, Li^+, and Water along the Liquid−Vapor Coexistence Curve

T (K)	ρ_w (g cm^{-3})	D_{H^+}	D_w (Å^2 ps^{-1})	D_{Li^+}
298.15	1.00	0.93[a]	0.21[b]	0.10[a]
373.15	0.96	2.1[c]	0.86[b]	0.4[c]
473.15	0.87	3.5[c]	2.4[d]	1.1[c]
573.15	0.72	4.5[c]	3.9[e]	2.0[c]
623.15	0.63	4.9[c]	5.1[e]	2.9[c]
673.15[g]	0.30	1.7[c]	11.2[f]	3.0[c]

[a] From ref 64. [b] From ref 65. [c] From ref 66. [d] From ref 67. [e] From ref 68. [f] From ref 69. [g] Corresponds to a supercritical temperature.

Proton Transport. The diffusion coefficient of aqueous protons at ambient conditions is known to be approximately a factor of 4 times larger than that observed for neat water. This difference rises to almost 1 order of magnitude when a similar comparison is established with a small cation such as Li^+. The large enhancement of proton mobility is normally ascribed to charge transport contributions from the Grotthus translocation mechanism,[10] in addition to the usual hydrodynamic Stokes mass diffusion.

A similar analysis performed in aqueous systems at elevated temperatures and lower densities shows interesting changes. In Table 2, we list experimental results for the diffusion coefficients of aqueous H^+, Li^+, and water covering a wide temperature range along the liquid−vapor coexistence curve. The results were obtained from conductometric measurements of aqueous solutions of HCl, LiCl, and KCl[62−66] by first estimating the individual ionic conductivities λ_M^o from:

(57) Borgis, D.; Tarjus, G.; Azzouz, H. *J. Chem. Phys.* **1992**, *97*, 1390.
(58) Laria, D.; Ciccotti, G.; Ferrario, M.; Kapral, R. *J. Chem. Phys.* **1992**, *97*, 378.
(59) Agmon, N. *Chem. Phys. Lett.* **1995**, *244*, 456.
(60) For a general review of the formalism see: Bolhius, P. G.; Dellago, C.; Chandler, D.; Geissler, P. *Annu. Rev. Phys. Chem.* **2002**, *53*, 291.
(61) In fact, changes in temperature also affect the temporal prefactor of the classical transition state theory expression for the rate that roughly scales as the square root of the ratio of temperatures, which in this case is $\sim\sqrt{2}$.
(62) Sansom, M. S. P.; Kerr, I. D.; Breed, J.; Sankararamakrishnan, R. *Biophys. J.* **1996**, *70*, 693.
(63) The agreement between the overall shapes of $\rho_{o*\alpha}(r)$ for single and multiple VB Hamiltonian pregressively worsens as we move to higher densities, and therefore the case $\rho_w = 1$ g cm^{-3} was not considered.
(64) Robinson, R. A.; Stokes, R. H. *Electrolyte Solutions*; Butterworths: London, 1959.
(65) Simpson, J. H.; Carr, H. Y. *Phys. Rev.* **1958**, *111*, 1201.
(66) (a) Ho, P. T.; Palmer, D. A.; Gruskiewicz, M. S. *J. Phys. Chem. B* **2001**, *105*, 1260. (b) Ho, P. T.; Bianchi, H.; Palmer, D. A.; Wood, R. H. *J. Sol. Chem.* **2000**, *29*, 217.

$$\lambda^{o}_{H^+} = \Lambda^{o}(HCl) - t_{-}\Lambda^{o}(KCl)$$
$$\lambda^{o}_{Li^+} = \Lambda^{o}(LiCl) - t_{-}\Lambda^{o}(KCl) \quad (11)$$

where $\Lambda^{o}(MX)$ represents the limiting molar conductivity of the MX electrolyte; t_{-} represents the transport number of Cl^{-} in the KCl solution that was taken as 0.5 for all the states considered.[67−70] From individual conductivities, diffusion coefficients can be readily obtained through Einstein's relationship:

$$D_i = \frac{\lambda^{o}_i}{\beta N_A e^2} \quad (12)$$

where N_A and e represent the Avogadro number and the charge of the electron, respectively. Note that as we move to higher temperatures and lower densities, the mobilities of the proton and water become more comparable, being practically identical at $T = 623$ K, $\rho_w = 0.63$ g cm^{-3}. Table 2 also includes one entry corresponding to the SC state $T = 673$ K, $\rho_w = 0.30$ g cm^{-3}. It is clear that the original, room-temperature trend is reversed: In moderate density SC environments, water molecules diffuse at least at 1 order of magnitude faster than protons, which in turn would migrate even slower than Li^+.

To shed light on the microscopic details of these changes, we have computed diffusion coefficients from the limiting slopes of the root mean square displacements of the proton coordinate $\mathbf{r}_p$, namely:[38]

$$D_{H^+} = \frac{1}{6}\lim_{t\to\infty}\frac{d}{dt}\langle|\mathbf{r}_p(t) - \mathbf{r}_p(0)|^2\rangle \quad (13)$$

In the last equation, the proton coordinate was defined as a weighted sum of the coordinates $\mathbf{r}^i_{pvt}$ corresponding to the L oxygen participating in the construction of $\hat{H}_{EVB}$, namely:

$$\mathbf{r}_p = \sum_{i=1}^{L} c_i^2\,\mathbf{r}^i_{pvt} \quad (14)$$

Results for the diffusion coefficients are shown in Table 1 along with those obtained for the TIP3P model (fifth and sixth columns, respectively). Interestingly, note that our simulation results reproduce the qualitative trends observed in the experiments: compared to pure water, the proton turns from a more mobile solute at high densities into a much slower particle at lower densities, with transport properties very much akin to those of a prototypical cation of a small size. The change in the diffusional regime of the proton suggests that the role of the Grotthus mechanism—as a key factor determining the abnormal, high proton conductivity—should become less important at low densities. A crude estimate of this contribution is normally obtained using simple random walk arguments as follows.[29,59] Results from NMR measurements show that at ambient conditions the proton jumps a characteristic O*−O distance, say ∼2.5 Å, every $\tau = 1-2$ ps.[71] During this time interval, the displacement of the center of mass of a water molecule is $l \approx (6D_w\tau)^{1/2} \approx 1.5-2$ Å. Consequently, the proton translocation mechanism increases the mobility in a sizable fashion. If we repeat a similar calculation for $T = 673$ K, $\rho_w = 0.1-0.05$ g cm^{-3} assuming that the rates of proton transfer do not vary substantially, the change in D_w (of almost 2 orders of magnitude) leads to $l \approx 15-20$ Å. Under these circumstances, the spatial displacement during proton translocation is much smaller when compared to that of the center of mass of water molecules operated by ordinary diffusion.

The previous description of proton transport is still incomplete since it is based solely on the simple picture of a diffusive water molecule plus a proton jump mechanism. The hydronium is a relatively small ionic species, and we have mentioned that important modifications take place in the structure of pure water to accommodate the solute; most notably, the presence of a first solvation shell composed of three strongly interacting water molecules that are dragged by the solute as it diffuses. The data of the fifth column of Table 1 show that the diffusion coefficients of the proton change very little along the high to mid-density interval, for example, 0.3 g cm$^{-3} \lesssim \rho_w \lesssim 1$ g cm^{-3}, before increasing somewhat more sharply, at lower densities. We wish to remark that this density insensitivity is not observed in this density interval for ordinary cations of comparable size such as Li^+ or Na^+. Thus, we tend to believe that it is the result of a cancellation between the natural reduction of the friction as we move down in density, compensated by a lesser extent of contributions to global mobility from the translocation mechanism.

To further validate this line of reasoning, we have performed a series of test runs using a surrogate model in which we eliminated the possibility of proton jumping by restricting the number of VB states to $L = 1$. The suppression of nondiagonal elements, however, leads to a hydrated H_3O^+ weakly coupled to the surroundings, as reflected, for example, in the resulting heights and widths of $\rho_{o^*o}(r)$, when compared to those obtained with multiple VB states. As a solution of direct implementation to enhance the coupling, we found that a rescaling in the partial charges of the pivot of up to $z_H = 0.7$, $z_O = (1-3z_H)$, and a modification in the parameter $D_{OH} = 466.0$ kcal mol^{-1} (see Table 1 of ref 36) were sufficient to maintain a similar coordination in the first shell, thus bringing the overall shapes and heights of the main peaks of $\rho_{o^*\alpha}(r)$ for single and multiple VB states to reasonable accordance in the mid- and low-density intervals.[63] Although we will not claim that this ad hoc, structural criterion is fully satisfactory in establishing a reference in singling out contributions to transport from the translocation mechanism, it seems more adequate than the simple suppression of nondiagonal terms in the Hamiltonian. Results for the diffusion coefficient of the hydronium using this crude, one-EVB model are displayed as $D^*_{H^+}$ in the last column of Table 1. The absence of jumping mechanisms leads to: (i) a reduction in the diffusion coefficient at the highest density, $\rho_w = 0.65$ g cm^{-3}, (ii) a somewhat more uniform density dependence of the diffusion, and (iii) reasonable estimates for the proton mobility

(67) Krynicki, K.; Green, C. D.; Sawyer, D. W. *Faraday Discuss. Chem. Soc.* **1979**, *66*, 199.
(68) Hausser, R.; Maier, G.; Noack, F. *Z. Naturforsch. A* **1966**, *21*, 1410.
(69) Lamb, W. J.; Hoffman, G. A.; Jonas, J. *J. Chem. Phys.* **1981**, *74*, 6875.
(70) Although this hypothesis is not strictly true, the errors up to $T = 573$ K are negligible. For more details, see: (a) Quist, A. S.; Marshall, W. L. *J. Phys. Chem.* **1965**, *69*, 2984. (b) Marshall, W. L. *J. Chem. Phys.* **1987**, *87*, 3639.
(71) (a) Meiboom, S. *J. Chem. Phys.* **1961**, *34*, 375. (b) Herzt, H. G.; Manner, R. *Z. Phys. Chem. (Munich)* **1983**, *135*, 89. (c) Pfeifer, R.; Hertz, H. G. *Ber. Bunsen-Ges. Phys. Chem.* **1990**, *94*, 4, 1349.

at low densities, confirming that under these conditions, contributions from the Grotthus mechanism to the transport are negligible.

Proton Spectroscopy. Before closing this section we will comment on the main features pertaining to the vibrational spectroscopy of aqueous protons at elevated temperatures. The infrared absorption line shape can be readily obtained from the Fourier transform of the time correlation function of the time derivative of the dipole moment,[42,72]

$$I(\omega) \propto \int_0^\infty \exp(-i\omega t)\, \langle \dot{\boldsymbol{\mu}}(t)\cdot\dot{\boldsymbol{\mu}}(0)\rangle \, \mathrm{d}t \qquad (15)$$

Within the EVB framework, the time derivative of the dipole moment shown in the integrand of eq 15 includes contributions from nuclear velocities as well as polarization fluctuations:[42,72]

$$\dot{\boldsymbol{\mu}}(t) = \sum_i q_i(t)\dot{\mathbf{R}}_i(t) + \sum_i \dot{q}_i(t)\mathbf{R}_i(t) \qquad (16)$$

In the previous equation, $q_i(t)$ denotes a weighted sum of the partial charges of site i, computed as:

$$q_i(t) = \sum_j c_j^2(t) q_i^j \qquad (17)$$

where q_i^j represents the charge of site i participating in the jth VB state. To compute the dipole moment and its time derivative, we considered contributions exclusively from the six instantaneous VB states exhibiting the largest weights c_i^2. Estimates for the time derivatives of the coefficients c_i were obtained from standard first-order perturbation theories, in accordance to:[73]

$$\dot{c}_i = \sum_{j\neq 0} \frac{1}{\epsilon_j - \epsilon_0} \Big(\sum_k \nabla_{\mathbf{R}_k} h_{j0}\cdot\dot{\mathbf{R}}_k\Big)\langle\phi_i|\psi_j\rangle \qquad (18)$$

Results for the two limiting SC states, i.e., $\rho_w = 1$ and 0.05 g cm^{-3}, are shown in Figure 5. Similar to what one finds in results for room temperature, the signature of excess protons in SC water is given by continuum bands in the 1500−3500 cm^{-1} frequency interval. In pure water at ambient and SC conditions, this frequency domain, which is flanked by the bending and the O−H stretching bands, appears deprived of any relevant feature. The resolution of this band at ambient conditions shows absorption maxima located at 1500−1600 cm^{-1} and 2900−3000 cm^{-1}.[72] This original structure gets considerably rippled and broadened when one considers aqueous states at elevated temperatures. Anyhow, our simulations predict that at high densities, proton absorption is dominated by a peak at 2450−2500 cm^{-1} and, possibly, by a much smaller second one located in the 1900−2000 cm^{-1} region. At low densities, the more noticeable change operates in the high-frequency peak that gets broadened and presents a moderate 200 cm^{-1} blue-shift.

A description of the underlying proton dynamics and the possibility of establishing a correspondence between these profiles and the one obtained at room temperature is not straightforward since the vibrational modes are normally quite delocalized as well as coupled to degrees of freedom of the local environment.[74] In addition, due to the flatness in the potential energy profiles describing strong hydrogen bonds, the harmonic description of the dynamics may not always be satisfactory.[75,76] Still, an analysis based on vibrational contributions from Zundel and Eigen-like structures in vacuo can be instructive. In this context, the relevant cluster modes that are likely to be connected to the observed absorptions at SC conditions are the 1740−1780 asymmetric bending mode of the Zundel dimer[77,78] and the collective O−H stretch at 2660 cm^{-1} of the Eigen complex.[79,80] In the inset of Figure 5 we show the computed spectra for hot $[H_3O\cdot(H_2O)_3]^+$ and $[H\cdot(H_2O)_2]^+$ clusters at $T \approx 673$ K. Note that despite the elevated temperature, absorption remains located roughly within the frequency intervals found at room temperature.[36] As a possible interpretation of the overall SC line shapes, we tend to believe that the peaks located in the 1900−2000 cm^{-1} and 2450−2500 cm^{-1} regions are the results of different contributions from configurations with predominant Zundel and Eigen-like structures, respectively. Moreover, the blue-shift observed for $\rho_w = 0.05$ g cm^{-3} would be accordant with the gradual approach to $[H_3O\cdot(H_2O)_3]^+$ "cluster-like" structures that should prevail in steamlike environments.

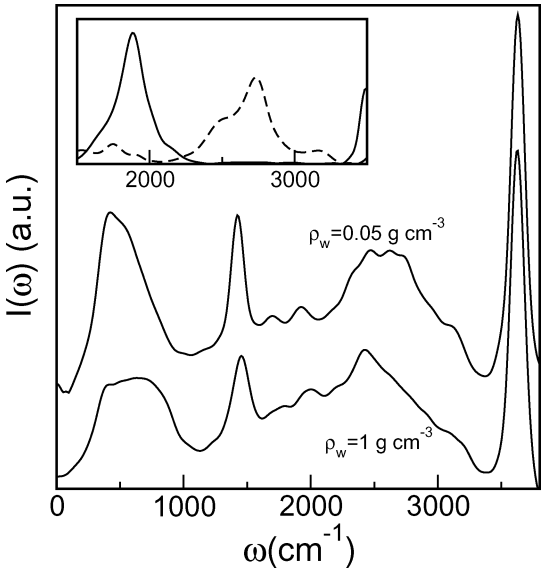

Figure 5. Absorption line shapes of protonated water for liquidlike and vaporlike aqueous SC environments. The inset shows the absorption line shapes for the Zundel dimer (solid line) and Eigen complex (dashed line) at 673 K in the frequency interval where the excess proton modes prevail.

Concluding Remarks

The results presented in this study provide new insights into microscopic details of the solvation of excess protons in supercritical states of water and can be summarized as follows. Our simulations predict a gradual stabilization of Eigen-like structures at low densities, in detriment of Zundel-like dimers. In contraposition to the usual tetrahedral coordination of the pure liquid, the first solvation shell of the hydronium is

(72) Kim, J.; Schmitt, U. W.; Gruetzmacher, J. A.; Voth, G. A.; Scherer, N. E. *J. Chem. Phys.* **2002**, *116*, 737.
(73) Vuilleumier, R. Ph.D. Thesis. University of Paris VI, 1998.
(74) Librovich, N. B.; Sakun, V. P.; Sokolov, N. D. *Chem. Phys.* **1979**, *39*, 351.
(75) Ojamäe, L.; Shavitt, I.; Singer, S. J. *Int. J. Quantum Chem., Symp.* **1995**, *29*, 657.
(76) Vener, M. V.; Kühn, O.; Sauer, J. *J. Chem. Phys.* **2001**, *114*, 240.
(77) Asmis, K. R.; Pivonka, N. L.; Santambrogio, G.; Brümmer, M.; Kaposta, C.; Neumark, D. M.; Wöste, L. *Science* **2003**, *299*, 1375.
(78) Yeh, L. I.; Myers, J. D.; Price, J. M.; Lee, Y. T. *J. Chem. Phys.* **1989**, *116*, 737.
(79) Schwarz, J. A. *J. Chem. Phys.* **1977**, *67*, 5525.
(80) Newton, M. D. *J. Chem. Phys.* **1977**, *67*, 5535.

characterized by three hydrogen-bond acceptor water molecules strongly interacting with the solute, with no neighboring water molecule acting as an eventual hydrogen bond donor. This structure persists along the whole range of fluid densities and shows a considerable enhancement of the local solvent density in the close vicinity of the solute at low densities.

From the dynamical point of view, the stabilization of the Eigen structure goes hand in hand with a sensible reduction of the rates for the proton transfer. A comparison between results from a typical steamlike state and from ambient conditions shows that the usual accelerating thermal effects are practically compensated by an opposite density trend which, as we move toward lower densities, promotes a sensible increase in the time scales characterizing the proton jump. These results suggest that important changes should also take place in the mechanism that drive the charge transport. In the high to mid-density range, the proton diffusion presents a plateaulike behavior, which can be ascribed to compensations between the natural reduction of friction and the lesser extent of displacements operated via proton translocations. At very low densities, our results predict that the proton migrates slower than water, which is in agreement with the experimental evidence. As such, proton transfers in steams can be pictured as more closely related to an "intramolecular process" within a diffusing Zundel-like complex than to a charge defect translocation along a tridimensional network of hydrogen bonded molecules. Consequently, there is no need to invoke proton jump mechanisms to obtain adequate estimates for the charge displacements. Moreover, the lesser extent of solvent hydrogen bond interconnectivity beyond the first solvation shell leads to a sensible reduction of the coupling between the proton and the fluctuating environment and would explain the reduction of the rate for the proton transfer. We finally remark that results from vibrational spectra of the proton in high-temperature liquid, and steamlike systems are accordant to the solvation stabilization of Eigen-like structures in the latter environments.

Of course, the analysis presented here is far from being complete, and there are several open questions of fundamental importance that will require further investigation. Eventual improvements on the parametrization of the EVB Hamiltonian is perhaps the first issue that will deserve attention. The transferable, three-point charge, water−water potential employed here belongs to a family of mean field models that have been extensively tested in numerous simulations of water, both at ambient and extreme conditions.[81−86] Simulation results at high temperatures usually show an overall trend toward somewhat more accentuated structures.[87] Some of these inadequacies can be avoided by resorting to more computationally demanding, ab initio molecular dynamics techniques that yield better descriptions of the water structure and the hydrogen bonding.[88]

It is important to remark that within the present EVB analysis, the particular choice of the water Hamiltonian will affect in sensible fashion the magnitude of the coupling between EVB Hamiltonian and the polarization fluctuations provided by the classical bath. These fluctuations will be most likely enhanced in dilute gas phases, since mean field models are originally adjusted to describe the dipole moment of water at ambient conditions $\mu \approx 2.5$ D, which is larger than the dipole moment of water of the isolated water molecule, $\mu = 1.85$ D. Yet, we still believe that the overall qualitative performance of the flexible TIP3P Hamiltonian employed is sufficient to yield a realistic description of water over a wide region of its phase diagram, including the supercritical interval of interest in this work.

The particular parametrization of the diagonal and nondiagonal elements of the EVB Hamiltonian matrix, originally tailored to reproduce quantum results for the energetics, geometries, and vibrational frequencies of clusters of the types $H_5O_2^+$, $H_7O_3^+$, and $H_9O_4^+$, could in principle raise some additional concerns. In this respect, we do not foresee major drawbacks since the energetics and the solvation structure of charged species in low density aqueous systems should be dominated by a considerable extent of solvent clustering in the close vicinity of the solute.

Particularly important will be to further examine whether the microscopic mechanisms that drive the proton transfer at ambient conditions present modifications at high-temperature, low-density aqueous states. The answer to this question does not seem straightforward and will require a physical interpretation of the slower rates found at low densities in terms of the usually faster relaxations of the relevant processes, most notably, the lifetimes of hydrogen bonds and/or individual and collective orientational modes, which are likely to control the transfer mechanism. Moreover, the observed modifications in the proton rates, along with the absence of any relevant structural changes in the first solvation shell, would suggest that the collective modes that trigger the transfer are to be found in the second solvation shell or beyond.

An additional analysis of the role of quantum fluctuations at high temperatures is also relevant. At ambient conditions, quantum effects on the hydration structure are translated into a considerable extent of spatial delocalization of the charge defect[13] and overestimations in the stability of Eigen-like structures. On the other hand, from the dynamical side, a classical treatment for the proton leads to an enhancements in the free energy barriers associated with the proton jump,[13,36] thus lowering the rates for proton transfer and reducing proton diffusion.[36,42] Anyhow, although a precise assessment is surely called for, invoking basic statistical mechanics arguments and on the basis of the physical picture of the proton transport provided here, one should expect that quantum effects on the rates and on the proton diffusion at elevated temperatures should be somewhat milder than those already found at room temperature. Research along these lines is currently being carried out in our laboratory and will be the subject of a forthcoming publication.

Finally, it would have been highly desirable if the arguments presented in the previous paragraphs could be supported by additional experimental information. Unfortunately, due to a

(81) Jedlovsky, P.; Brodholt, J. P.; Brin, F.; Ricci, M. A.; Soper, A. K.; Vallauri, R. *J. Chem. Phys.* **1998**, *108*, 8528.
(82) Liew, C. C.; Inomata, H.; Arai, K. *Fluid Phase Equilib.* **1998**, *144*, 287.
(83) Bellissent-Funel, M.-C.; Tassaing, T.; Zhao, H.; Beysens, D.; Guillot, B.; Guissani, Y. *J. Chem. Phys.* **1997**, *107*, 2942.
(84) Mizan, T. I.; Savage, P. E.; Ziff, R. M. *J. Phys. Chem.* **1994**, *98*, 10367.
(85) Martí, J. *J. Chem. Phys.* **1999**, *110*, 6287.
(86) Boulougouris, G. C.; Economou, I. G.; Theodorou, D. N. *J. Phys. Chem. B* **1998**, *102*, 1029.
(87) For a recent review article on the performance of different water Hamitonians, see: Guillot, B. *J. Mol. Liq.* **2002**, *101*, 219.
(88) Boero, M.; Terakura, K.; Ikeshoji, T.; Liew, C. C.; Parrinello, M. *J. Chem. Phys.* **2001**, *115*, 2219.

large number of technical difficulties, thermodynamic information of high-temperature solutions still remains rather scarce. This situation underlines the importance of simulation studies as a useful guidance to gain physical insight into solution chemistry at extreme conditions of temperature and pressure. The similarities found between the experimental and simulated overall trends for proton diffusion seem to corroborate that the model implemented here is able to retain the essential ingredients that drive the proton transport at high temperatures. We hope that our conclusions act as motivation in sparking interest to perform new experimental measurements that may provide support to the physical picture presented here.

Acknowledgment. We gratefully acknowledge financial support from the Secretaría de Educación y Universidades de España, the Direcció General de Recerca de la Generalitat de Catalunya (Grant 2001SGR-00222), and the Ministerio de Educación y Cultura Deporte de España (Grant BFM2000-0596-C03-02). D.L. is a member of Carrera del Investigador Científico de CONICET (Argentina).

JA0373418